Single-Mode Phononic Wire

Rishi N. Patel,[*] Zhaoyou Wang, Wentao Jiang, Christopher J. Sarabalis, Jeff T. Hill, and Amir H. Safavi-Naeini[†]

Department of Applied Physics and Ginzton Laboratory, Stanford University, 348 Via Pueblo Mall, Stanford, California 94305, USA

Photons and electrons transmit information to form complex systems and networks. Phonons on the other hand, the quanta of mechanical motion, are often considered only as carriers of thermal energy. Nonetheless, their flow can also be molded in fabricated nanoscale circuits. We design and experimentally demonstrate wires for phonons by patterning the surface of a silicon chip. Our device eliminates all but one channel of phonon conduction, allowing coherent phonon transport over millimeter length scales. We characterize the phononic wire optically, by coupling it strongly to an optomechanical transducer. The phononic wire enables new ways to manipulate information and energy on a chip. In particular, our result is an important step towards realizing on-chip phonon networks, in which quantum information is transmitted between nodes via phonons.

Engineered structures guide waves of light, sound, and electrons—transmitting information and energy across distances from microns to kilometers. The most prominent examples are the optical waveguides that form the physical basis of the internet, integrated photonic technologies [1], nonlinear optics [2], and the emerging quantum internet [3–5]. The mechanical analog of these electromagnetic structures are *phononic wires* or *waveguides* that would coherently transport mechanical energy and information in highly confined waves. Currently established approaches for guiding mechanical waves over many wavelengths use surface or bulk acoustic waves that are unconfined in the direction transverse to propagation [6–9]. Attempting to confine these waves leads to large scattering and diffractive losses and prevents the development of complex phononic circuitry and confinement-enhanced interactions. Additionally, highly confined mechanical waveguides are difficult to excite electromagnetically by direct capacitive or piezoelectric coupling due to the vanishing capacitance of small transducers. In this work, we address these challenges by realizing a single-mode phononic wire. We observe low-loss coherent phonon transport of highly confined phonons over millimeter length scales at cryogenic temperatures. Furthermore, we demonstrate an efficient means to excite and detect phonons in the wire using an optomechanical transducer that realizes highly efficient readout of the guided modes. Our work takes a key step towards realizing phonon networks such as those recently proposed to distribute quantum information on a chip [10–12].

Phonon conduction in a quantum wire can occur through four independent channels [13]. These channels correspond to two flexural excitations, a dilatational, and a torsional wave. All channels persist in the long-wavelength limit down to zero frequency. The existence of multiple polarizations complicates phonon transport over long distances since small amounts of disorder lead to interchannel scattering and a rapid loss of coherence. This scattering makes the response of the system sensitive to details, reminiscent of quantum chaos in mesoscopic samples [14,15]. Moreover, interchannel scattering is enhanced by going to highly confining structures as needed to push higher-order phonon conduction channels into cutoff.

We overcome these challenges by nanoscale patterning of phononic materials. Phononic crystals use periodicity to significantly modify the mode spectrum for mechanical waves [16,17]. The most dramatic effect is the elimination of phonons of all polarizations for a given range of frequencies by formation of a full phononic band gap [18,19]. We induce a line defect on a phononic crystal possessing a full band gap to generate a structure where only a single propagating mode of group velocity $v_g \approx$ 6800 m/s is allowed within a large range of frequencies [Fig. 1(a)]. The waveguide is fabricated in a suspended film of silicon with thickness 220 nm using a combination of *e*-beam lithography, and dry and wet etching [20].

We use techniques from cavity optomechanics to transduce propagating waves within the phononic wire. A nanoscale cavity optomechanical resonator, in which a high-Q optical cavity is dispersively coupled to a mechanical mode, is fabricated adjacent to the waveguide structure. The device has an optical cavity resonance near $\lambda_c =$ 1560 nm (with annihilation operator $\hat{a}$) and a mechanical resonance near $\omega_m/2\pi = 4.4$ GHz (with annihilation operator $\hat{b}$). The interaction between these modes is described by $\hat{H}_{int} = \hbar g_0 \hat{a}^\dagger \hat{a}(\hat{b} + \hat{b}^\dagger)$, where g_0 denotes the frequency jitter of the optical resonator due to the zero-point-motion of the mechanical resonator. In our experiment, optical photons are used to read out and control the motion of the localized phonon mode $\hat{b}$. By engineering controlled
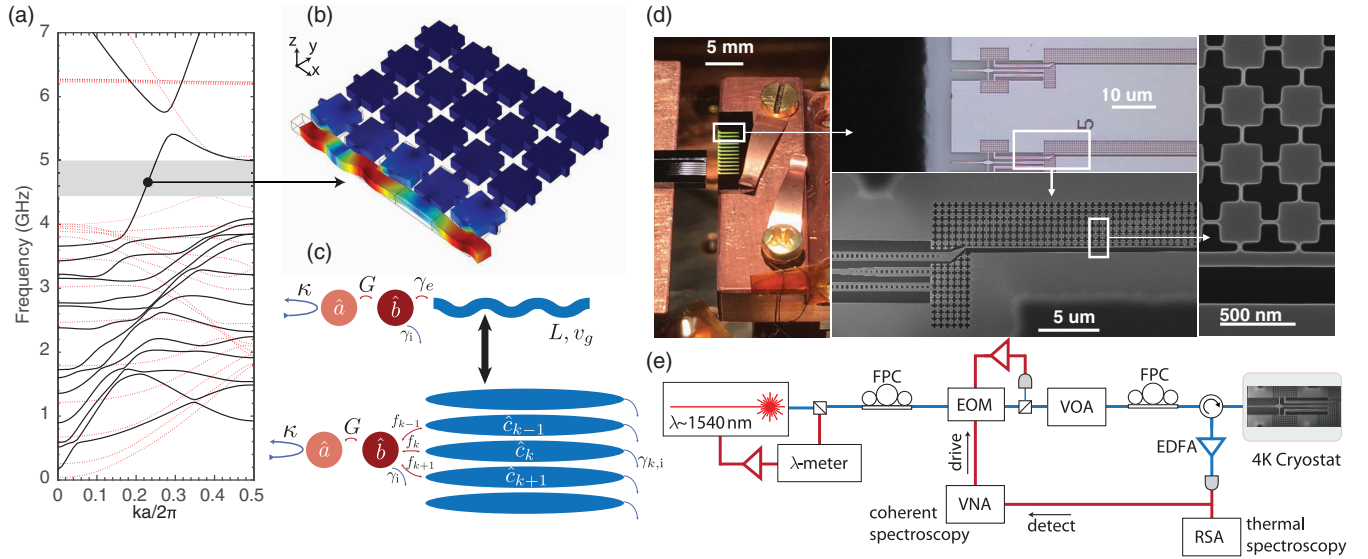
FIG. 1. System concept and experiment overview. (a) Band diagram for the single-mode phonon waveguide. The solid black (dotted-red) lines show the z-symmetric (antisymmetric) bands, respectively. The single-mode region is shaded. (b) Simulated displacement field for a longitudinal edge mode in the band gap. (c) Concept of the readout mechanism, showing an optical mode $\hat{a}$ (with loss rate κ), coupled to a localized mechanical resonance $\hat{b}$ (with loss rate γ_{i}) at a rate G. The localized mechanical mode is coupled to a terminated single-mode waveguide at rate γ_e. On the bottom is an equivalent picture, treating each waveguide mode as a standing wave coupled at a rate f_k (with loss rate $\gamma_{k,\mathrm{i}}$). (d) The cryostat setup, a laser confocal image of the device, and two scanning electron micrographs. (e) Simplified diagram of the optical setup. A laser probes an optomechanical cavity in reflection. Electro-optic modulator (EOM), variable optical attenuator (VOA), erbium-doped fiber amplifier (EDFA), vector network analyzer (VNA), realtime spectrum analyzer (RSA), fiber polarization controller (FPC).

phonon leakage of the localized mechanical resonator, we achieve optical readout of phononic wire modes.

As shown in Fig. 1(c) a phonon waveguide of length L, which supports traveling waves of group velocity v_{g}, can be considered as an extended acoustic cavity that supports standing-wave modes. Each extended mode of the wire, indexed by k, is coupled to the localized mechanical resonance of the transducer at a rate f_k. The coupling between the extended modes and the transducer mode is given by

$$\hat{H}_{\mathrm{wg,int}} = \sum_k \hbar f_k (\hat{c}_k^{\dagger}\hat{b} + \hat{b}^{\dagger}\hat{c}_k), \qquad (1)$$

where we take f_k to be real, and operators $\hat{c}_k$ annihilate phonons in the kth standing-wave mode of the wire. To optically read out phonons in the localized transducer, we drive the system with a laser whose frequency is lower than the cavity frequency by an amount ω_{m}. Under this condition, and considering that the optical linewidth κ is smaller than ω_{m}, the optomechanical interaction is described by a linearized beam splitter Hamiltonian: $\hat{H}_{\mathrm{int}} = \hbar G(\hat{a}^{\dagger}\hat{b} + \hat{b}^{\dagger}\hat{a})$, where $G = g_0\sqrt{n_{\mathrm{c}}}$ is the laser-enhanced optomechanical coupling rate for n_{c} pump photons [21]. Any optical interaction with the phonon waveguide modes $\hat{c}_k$ occurs through the transducer mode $\hat{b}$, and is therefore enhanced near the mechanical resonance at frequency ω_{m}.

A simplified diagram of the experimental setup used to perform low-temperature ($T = 11$ K) coherent and thermal spectroscopy is shown in Fig. 1(e). In coherent spectroscopy, in addition to the strong pump described above, we generate a weak probe tone that is swept across the cavity resonance. The probe experiences a large phase shift at pump-probe detunings near the mechanical resonances of the structure. This is a generalization of electromagnetically induced transparency (EIT) for optomechanical systems [22–25]. Separately, the incoherent spectrum of the thermal phonons scattered into a sideband of the optical pump field is measured by analyzing the power spectral density of the detected light field. The thermal spectrum of an optomechanical transducer uncoupled from a phononic wire would have a Lorentzian line shape centered at the mechanical frequency, arising from losses into a nearly Markovian bath. In contrast, the phononic wire acts as a strongly non-Markovian bath and modifies this detected spectrum leading to the emergence of multiple peaks as shown in Fig. 2(a).

The results of thermal spectroscopy performed on two separate transducer modes with frequencies separated by 200 MHz are presented by the red and blue solid lines in Fig. 2. During fabrication, we sweep the phononic wire lattice constant over an 8% range, shifting the single-mode region of the wires across the frequencies of the two localized readout modes [Fig. 2(b)]. For each device, we record the normalized thermal spectrum as shown in
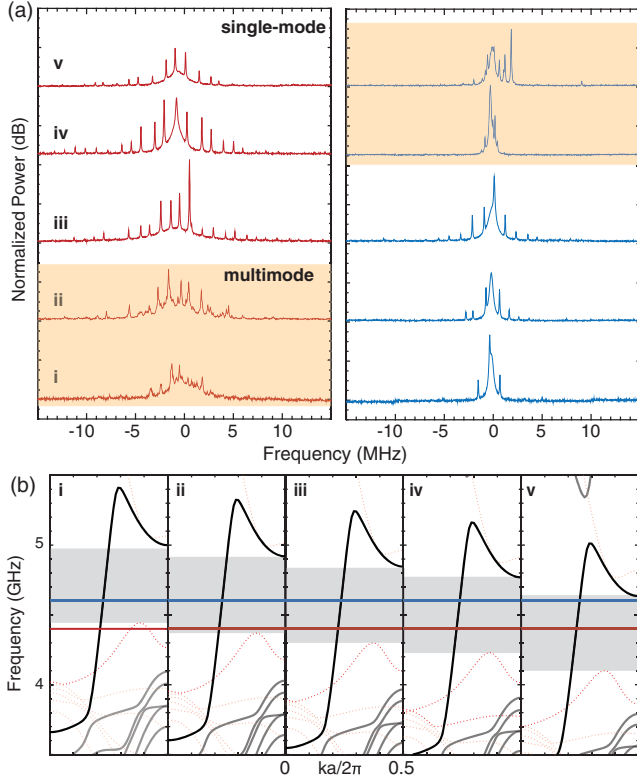
FIG. 2. Probing the single mode regime via structural tuning. (a) Experimentally measured thermal power spectra of the waveguide-cavity device as the lattice constant a is changed across five different devices, increasing from bottom to top. The left (right) sides show the spectra from localized readout mode 1 (2), respectively. $\omega_{m,1}/2\pi \approx 4.4$ and $\omega_{m,2}/2\pi \approx 4.6$ GHz. Labels denote $a = 450(i)$, $457(ii)$, $464(iii)$, $472(iv)$, and 486 nm(v). Shaded plots are multimode. (b) Band diagram of the waveguide for each lattice constant, with band gap denoted in gray. Horizontal lines show frequencies of the two transducer modes.

Fig. 2(a). The single-mode operation regime shows regularly spaced peaks on top of the broad thermal noise pedestal of the transducer signal [Fig. 2(a),iii]. The thermal spectra corresponding to multiband propagation are qualitatively different—they do not have a well-defined free spectral range (FSR) due to mixing between different phonon propagation channels [Fig. 2(a), i and ii]. In the single-mode case we determine an average mode spacing $\overline{\Delta\omega_k}/2\pi = 1.1 \pm 0.2$ MHz, agreeing with the expected FSR of $v_g/2L = 1.14$ MHz (with $L = 3$ mm). This corresponds to a round-trip time of approximately 900 ns.

We turn our attention to a device (where $L = 2$ mm) operating in the single-mode regime that is well represented by the model shown in Fig. 1(c) and in Eq. (1). Using coherent spectroscopy, we measure the frequency-dependent phase shift of the reflected probe, shown in Fig. 3. The force generated by the pump-probe interaction in the optomechanical transducer excites the phononic wire and leads to a significant modification of the probe response. The full system response is captured by a probe reflection coefficient derived from Eq. (1) and the optomechanical interaction Hamiltonian (for details see Supplemental Material [26]). The system parameters are estimated by fitting the theoretical phase response to the measured response. Here, the intracavity photon number n_c is independently measured at five different pump powers ranging from $P = 43$ to $P = 254$ μW, and our model is constrained by fitting to all five data sets simultaneously. We find good agreement between the data and the model with estimated waveguide mode coupling rates f_k, and intrinsic losses $\gamma_{k,i}$ [Fig. 3(c)]. In addition, the estimated parameters are consistent with simulations and previous measurements of intrinsic mechanical losses [20]. The average frequency spacing
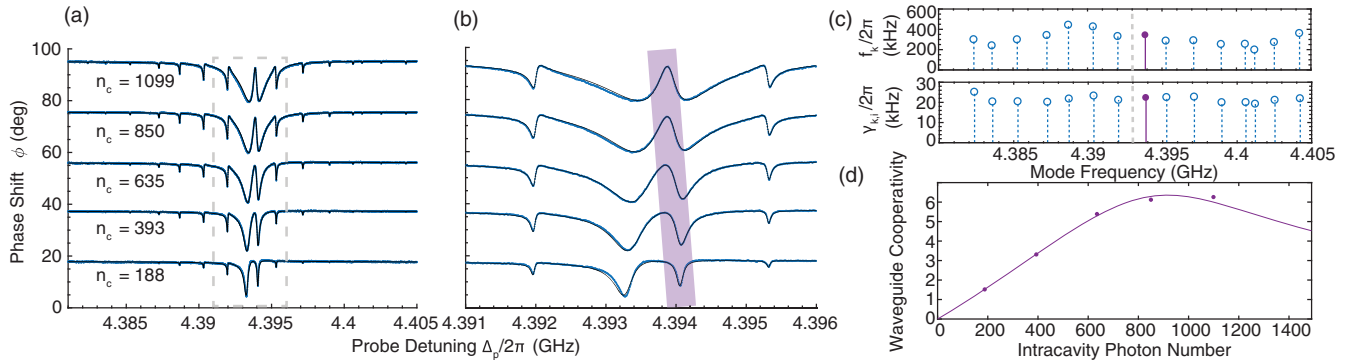

FIG. 3. Coherent linear spectroscopy results. (a) Phase response of a weak coherent probe tone as a function of detuning from the pump beam. Several coupled waveguide resonances are seen. The central dip broadens with laser power, due to sideband cooling of the localized mechanical mode. The black line is a fit to a theoretical model, described in the main text. (b) An enlargement of data from (a). The localized mode that is strongly mixed with the waveguide mode is highlighted in purple. (c) Model parameters estimated from the data set in (a), showing the waveguide-coupling rates f_k (top) and the intrinsic loss rates $\gamma_{k,i}$ (bottom) vs waveguide mode frequency. The gray dashed line shows the approximate frequency of the localized mechanical resonance. (d) Waveguide cooperativity inferred from model parameters for the mode highlighted in (b).

between modes, $\overline{\Delta\omega_k}/2\pi = 1.6 \pm 0.2$ MHz, agrees with an expected FSR ($v_g/2L = 1.7$ MHz) for the 2-mm-long phononic wire. Using the relation $f_k = \sqrt{\omega_{\text{FSR}}\gamma_e/2\pi}$, we find that the extrinsic mechanical loss rate, coupling the localized resonator to the waveguide, is $\gamma_e/2\pi = 386$ kHz, exceeding its intrinsic damping by more than an order of magnitude.

In our phase response data we observe broadening of the transducer mode, the broad resonance of Fig. 3(a), with increased optical power. This additional damping, given by $\gamma_{\text{OM}} = 4g_0^2 n_c/\kappa$, is the optical measurement rate of localized phonons [27]. In addition, in Fig. 3(b) we observe linewidth broadening of the waveguide resonances with increasing power. The total waveguide linewidth is defined as $\gamma_k = \gamma_{k,\text{i}} + \gamma_{k,\text{S}}$ where the first contribution is from intrinsic damping, and the second, power dependent contribution, is from optically induced damping. We define waveguide mode cooperativity as $C_{\text{wg}} = \gamma_{k,\text{S}}/\gamma_{k,\text{i}}$. A cooperativity larger than 1 represents coupling of an extended mode to the optical readout channel that is stronger than its intrinsic damping. In this regime, the waveguide modes undergo *sympathetic cooling*, in analogy to recent experiments in atomic physics [28]. C_{wg} is plotted in Fig. 3(d). We reach the large cooperativity regime, $C_{\text{wg}} > 1$ for the near-resonant waveguide mode. The peak cooperativity achieved is $C_{\text{wg}} \approx 6.3$ for an extended mode detuned by $\delta_k/2\pi \approx 630$ kHz from the localized transducer resonance. In contrast to a typical optomechanical system where the cooling rate increases linearly with input laser power, the extended mode cooperativity may display nonmonotonic behavior. The sympathetic cooling rate in the weak coupling limit $f_k \ll \gamma_{\text{OM}} \ll \kappa$ is $\gamma_{k,\text{S}} \approx |f_k|^2 \gamma_{\text{OM}}/(\delta_k^2 + \gamma_{\text{OM}}^2)$. At low optical power ($\gamma_{\text{OM}} \ll \delta_k$), increasing pump intensity leads to increased damping of the extended mode since the transducer mechanical response covers a broader bandwidth. At higher optical powers ($\delta_k \ll \gamma_{\text{OM}}$), we reduce the total quality factor of the transducer resonance, diminishing the readout rate in a manner analogous to a reduced Purcell enhancement.

The calibrated noise power spectrum for the same device is shown in Fig. 4(a). The black line in Fig. 4(a) is a fit to theory, using independent system parameters determined from our coherent spectroscopy results. The mode occupancy for both the localized and the extended modes are calculated from the measured noise powers [Fig. 4(b)]. We observe optical cooling of the extended modes of the phononic wire. The minimum waveguide mode phonon occupancy achieved is $n_{\text{phon}} = 42 \pm 4$, a factor of 2 below the intrinsic bath occupancy of $n_i = 87 \pm 11$. This intrinsic bath occupancy, denoted by the gray band in Fig. 4(b) and measured at low power across many devices [27] in the same experimental run, is smaller than the occupancy of detuned extended modes. For the extended mode nearly resonant with the transducer, the factor of 2 cooling
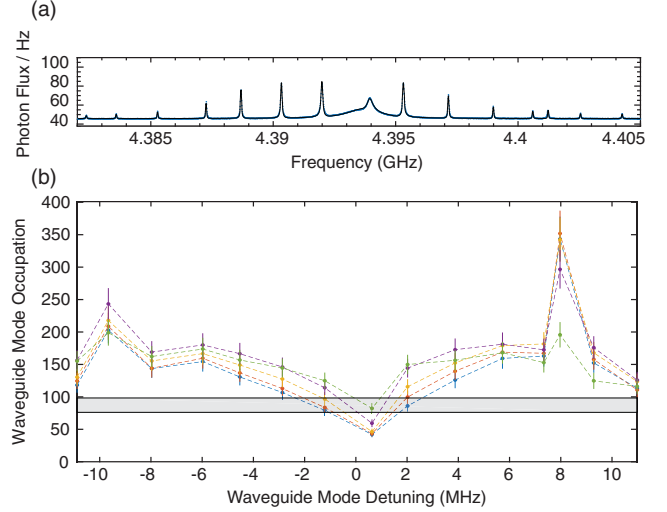

FIG. 4. Thermal spectroscopy and signatures of multimode cooling. (a) Experimental results showing the total thermal noise detected on reflection. Data points are shown in blue. The black line is a fit to theory with waveguide parameters fixed from coherent spectroscopy. (b) Extracted bath occupancies from the model showing cooling near resonance. The blue, red, yellow, purple, and green correspond to intracavity photon numbers 1099, 850, 635, 393, and 188, respectively. The gray band shows 1 standard deviation uncertainty in the intrinsic phonon bath occupancy. Error bars denote 10 percent error in the system gain estimate.

achieved is 3 times less than that estimated from $C_{\text{wg}} \approx 6$, due to optical absorption induced heating of the waveguide.

In addition to optical absorption, two other nonidealities of the phononic waveguide are loss and fabrication disorder. A simple estimate for the phonon loss rate per unit length is given by $\alpha_m = \gamma_{k,\text{i}}/v_g \approx 0.88$ dB/cm, values comparable to silicon photonic wires [29,30]. This loss is likely thermally activated by nonlinear phonon processes and α_m would be orders of magnitude smaller at lower temperatures (10 mK) [31]. For large classical signals at 10 K, we estimate a propagation distance of $L_{\text{3dB,c}} \approx 3$ cm. At the 10 K temperature, the injection of thermal phonons from the bath leads to a more rapid decoherence of quantum signals of roughly $\alpha_{\text{m,th}} = (n_i + 1)\gamma_{k,\text{i}}/v_g$ and a phonon being injected into the phononic wire after $L_{\text{3dB,q}} \approx 0.5$ mm of propagation. This decoherence would also be far smaller at 10 mK temperatures.

To faithfully transmit information along a wire, we must also consider the effect of disorder. Using a disordered tight-binding model of the waveguide we simulate both the single and multiband case and find that most of the features of the thermal and coherent spectra and resulting waveguide parameters can be reproduced theoretically for levels of disorder consistent with experiment. The measured disorder in the waveguide, i.e., the distribution of $\Delta\omega_k$, allows us to estimate the dephasing of an itinerant

excitation propagating in the phononic wire caused by random and static frequency-dependent phase shifts (see Supplemental Material [26]). This dephasing limits transmission to $L_{3dB,\delta} \approx 6$ mm.

Our demonstration of single-channel conduction of highly confined phonons is an important step in the development of phononic systems. The techniques of quantum optomechanics give us a powerful toolbox for manipulating propagating phonons on the surface of a chip. We have shown that optomechanical systems allow cooling and control of phononic circuits. In turn, the phononic guided wave structures can enhance optomechanical experiments by connecting elements spaced by millimeters, for example, in mechanically mediated microwave-to-optical converters [32–34] and phonon routers [35]. Though we have focused on linear ballistic phonon transport, applications to engineering heat flow in nonlinear structures are also possible [36]. Finally, the demonstrated mechanical waves have 3 to 5 orders of magnitude higher confinement than surface and bulk acoustic waves in the same frequency range, opening the way to the study of phonon-coupled emitters [37–39], two-level systems [40], and other phonon nonlinearities.

[*] rishipat@stanford.edu

[†] safavi@stanford.edu

[1] R. Soref, IEEE J. Sel. Topics Quant. Electron. **12,** 1678 (2006).

[2] R. W. Boyd, *Nonlinear Optics* (Academic Press, New York, 2003).

[3] H. J. Kimble, Nature (London) **453,** 1023 (2008).

[4] P. Lodahl, S. Mahmoodian, S. Stobbe, A. Rauschenbeutel, P. Schneewiss, J. Volz, H. Pichler, and P. Zoller, Nature (London) **541,** 473 (2017).

[5] D. Reitz, C. Sayrin, R. Mitsch, P. Schneewiss, and A. Rauschenbeutel, Phys. Rev. Lett. **110,** 243603 (2013).

[6] M. V. Gustafsson, P. V. Santos, G. Johansson, and P. Delsing, Nat. Phys. **8,** 338 (2012).

[7] A. D. O'Connell, M. Hofheinz, M. Ansmann, R. C. Bialczak, M. Lenander, E. Lucero, M. Neeley, D. Sank, H. Wang, M. Weides, J. Wenner, J. M. Martinis, and A. N. Cleland, Nature (London) **464,** 697 (2010).

[8] Y. Chu, P. Kharel, W. H. Renninger, L. D. Burkhart, L. Frunzio, P. T. Rakich, and R. J. Schoelkopf, Science **358,** 199 (2017).

[9] X. Han, C.-L. Zou, and H. X. Tang, Phys. Rev. Lett. **117,** 123603 (2016).

[10] S. J. M. Habraken, K. Stannigel, M. D. Lukin, P. Zoller, and P. Rabl, New J. Phys. **14,** 115004 (2012).

[11] B. Vermersch, P. O. Guimond, H. Pichler, and P. Zoller, Phys. Rev. Lett. **118,** 133601 (2017).

[12] M.-A. Lemonde, S. Meesala, A. Sipahigil, M. J. A Schuetz, M. D. Lukin, M. Loncar, and P. Rabl, Phys. Rev. Lett. **120,** 213603 (2018).

[13] K. Schwab, E. A. Henriksen, J. M. Worlock, and M. L. Roukes, Nature (London) **404,** 974 (2000).

[14] C. M. Marcus, A. J. Rimberg, R. M. Westervelt, P. F. Hopkins, and A. C. Gossard, Phys. Rev. Lett. **69,** 506 (1992).

[15] H. U. Baranger, R. A. Jalabert, and A. D. Stone, Phys. Rev. Lett. **70,** 3876 (1993).

[16] M. Maldovan, Nature (London) **503,** 209 (2013).

[17] D. Hatanaka, I. Mahboob, K. Onomitsu, and H. Yamaguchi, Nat. Nanotechnol. **9,** 520 (2014).

[18] J. Chan, A. H. Safavi-Naeini, J. T. Hill, S. Meenehan, and O. Painter, Appl. Phys. Lett. **101,** 081115 (2012).

[19] A. H. Safavi-Naeini and O. Painter, in *Cavity Optomechanics*, Quantum Science and Technology, edited by M. Aspelmeyer, T. J. Kippenberg, and F. Marquardt (Springer, Berlin, Heidelberg, 2014), p. 195.

[20] R. N. Patel, C. J. Sarabalis, W. Jiang, J. T. Hill, and A. H. Safavi-Naeini, Phys. Rev. Applied **8,** 041001 (2017).

[21] M. Aspelmeyer, T. J. Kippenberg, and F. Marquardt, Rev. Mod. Phys. **86,** 1391 (2014).

[22] S. Weis, R. Rivière, S. Deléglise, E. Gavartin, O. Arcizet, A. Schliesser, and T. J. Kippenberg, Science **330,** 1520 (2010).

[23] A. H. Safavi-Naeini, T. P. M. Alegre, J. Chan, M. Eichenfield, M. Winger, Q. Lin, J. T. Hill, D. Chang, and O. Painter, Nature (London) **472,** 69 (2011).

[24] F. Massel, S. U. Cho, J.-M. Pirkkalainen, P. J. Hakonen, T. T. Heikkilä, and M. A. Sillanpää, Nat. Commun. **3,** 987 (2012).

[25] A. H. Safavi-Naeini, J. T. Hill, S. Meenehan, J. Chan, S. Gröblacher, and O. Painter, Phys. Rev. Lett. **112,** 153603 (2014).

[26] See Supplemental Material at http://link.aps.org/supplemental/10.1103/PhysRevLett.121.040501 for theoretical derivations and detailed experimental methods.

[27] J. Chan, T. P. M. Alegre, A. H. Safavi-Naeini, J. T. Hill, A. Krause, S. Groblacher, M. Aspelmeyer, and O. Painter, Nature (London) **478,** 89 (2011).

[28] A. Jockel, A. Faber, T. Kampschulte, M. Korppi, M. T. Rakher, and P. Treutlein, Nat. Nanotechnol. **10,** 55 (2015).

[29] W. Bogaerts, R. Baets, P. Dumon, V. Wiaux, S. Beckx, D. Taillaert, B. Luyssaert, J. V. Campenhout, P. Bienstman, and D. V. Thourhout, J. Lightwave Technol. **23,** 401 (2005).

[30] R. Van Laer, B. Kuyken, D. Van Thourhout, and R. Baets, Nat. Photonics **9,** 199 (2015).

[31] S. M. Meenehan, J. D. Cohen, S. Gröblacher, J. T. Hill, A. H. Safavi-Naeini, M. Aspelmeyer, and O. Painter, Phys. Rev. A **90,** 011803 (2014).

[32] A. Vainsencher, K. J. Satzinger, G. A. Peairs, and A. N. Cleland, Appl. Phys. Lett. **109,** 033107 (2016).

[33] A. H. Safavi-Naeini and O. Painter, New J. Phys. **13,** 013017 (2011).

[34] K. C. Balram, M. I. Davanço, B. R. Ilic, J. H. Kyhm, J. D. Song, and K. Srinivasan, Phys. Rev. Applied **7,** 024008 (2017).

[35] K. Fang, M. H. Matheny, X. Luan, and O. Painter, Nat. Photonics **10,** 489 (2016).

[36] B. Li, L. Wang, and G. Casati, Phys. Rev. Lett. **93,** 184301 (2004).

[37] H. Pichler, S. Choi, P. Zoller, and M. D. Lukin, Proc. Natl. Acad. Sci. U.S.A. **114,** 11362 (2017).

[38] K. W. Lee, D. Lee, P. Ovartchaiyapong, J. Minguzzi, J. R. Maze, and A. C. Bleszynski Jayich, Phys. Rev. Applied **6,** 034005 (2016).

[39] P. Ovartchaiyapong, K. W. Lee, B. A. Myers, and A. C. B. Jayich, Nat. Commun. **5,** 4429 (2014).

[40] J. Suh, A. J. Weinstein, and K. C. Schwab, Appl. Phys. Lett. **103,** 052604 (2013).